Journal of Biomechanics 94 (2019) 75–81

Contents lists available at ScienceDirect

Journal of Biomechanics

journal homepage: www.elsevier.com/locate/jbiomech
www.JBiomech.com

Significance of preoperative planning for prophylactic augmentation of osteoporotic hip: A computational modeling study

Amirhossein Farvardin [a,b,*], Ehsan Basafa [c], Mahsan Bakhtiarinejad [a,b], Mehran Armand [a,b,d,e]

[a] Department of Mechanical Engineering, Johns Hopkins University, 3400 N Charles Street, Baltimore, MD 21218, USA
[b] Laboratory for Computational Sensing and Robotics, Johns Hopkins University, 3400 N Charles Street, Baltimore, MD 21218, USA
[c] Auris Health, Inc., 150 Shoreline Dr, Redwood City, CA 94065, USA
[d] Johns Hopkins University Applied Physics Laboratory, 11100 Johns Hopkins Rd, Laurel, MD 20723, USA
[e] Department of Orthopaedic Surgery, Johns Hopkins University, 601 N. Caroline Street, Baltimore, MD 21287, USA

ARTICLE INFO

Article history:
Accepted 11 July 2019

Keywords:
Osteoporotic hip augmentation
PMMA cement
Finite element analysis
Surgical planning

ABSTRACT

A potential effective treatment for prevention of osteoporotic hip fractures is augmentation of the mechanical properties of the femur by injecting it with bone cement. This therapy, however, is only in research stage and can benefit substantially from computational simulations to optimize the pattern of cement injection. Some studies have considered a patient-specific planning paradigm for Osteoporotic Hip Augmentation (OHA). Despite their biomechanical advantages, customized plans require advanced surgical systems for implementation. Other studies, therefore, have suggested a more generalized injection strategy. The goal of this study is to investigate as to whether the additional computational overhead of the patient-specific planning can significantly improve the bone strength as compared to the generalized injection strategies attempted in the literature. For this purpose, numerical models were developed from high resolution CT images (n = 4). Through finite element analysis and hydrodynamic simulations, we compared the biomechanical efficiency of the customized cement-based augmentation along with three generalized injection strategies developed previously. Two series of simulations were studied, one with homogeneous and one with inhomogeneous material properties for the osteoporotic bone. The customized cement-based augmentation inhomogeneous models showed that injection of only 10 ml of bone cement can significantly increase the yield load (79.6%, $P < 0.01$) and yield energy (199%, $P < 0.01$) of an osteoporotic femur. This increase is significantly higher than those of the generalized injections proposed previously (23.8% on average). Our findings suggest that OHA can significantly benefit from a patient-specific plan that determines the pattern and volume of the injected cement.

1. Introduction

The rate of mortality one year after osteoporotic hip fracture has been reported to be between 20% and 45% (e.g. Goldacre et al., 2002; Teng, 2008). Most of these fractures are due to low bone mass coupled with a fall to the side (e.g. Lane et al., 2000; Parkkari et al., 1999). A wealth of research on reducing fracture rates considers long-term preventive measures such as estrogens and selective estrogen receptor modulators, calcitonin, and bisphosphonates. The mentioned remedies, however, do not provide much-needed immediate prevention especially for elderly who have experienced a second fracture in the contralateral hip. The rate of second fracture occurrence is 6–10 times higher in patients who have already suffered an osteoporotic hip fracture (Dinah, 2002). Osteoporotic Hip Augmentation (OHA) with Polymethyl methacrylate (PMMA) bone cement is a potential treatment option for patients at the highest risk of fracture. Higher volumes of PMMA, however, may introduce the risk of thermal necrosis and other complications such as leakage or blockage of the blood support (Lundskog, 1972; Eriksson and Albrektsson, 1983). To this end, several cadaveric studies were conducted to investigate the efficiency and effectiveness of OHA using PMMA bone cement. Fliri et al. (2013) proposed a V-shaped cement pattern and showed that it results in an increased energy absorption until fracture. In the study of Beckman et al. (2011), it was concluded that a single central augmentation aligned with the femoral neck axis results in significant improvements in mechanical properties of the femur. Moreover, the patient-specific planning and computer-assisted

* Corresponding author at: 136 Hackerman Hall, Johns Hopkins University, 3400 N Charles Street, Baltimore, MD 21218, USA.
E-mail address: afarvar1@jhu.edu (A. Farvardin).

https://doi.org/10.1016/j.jbiomech.2019.07.012
0021-9290/

augmentation can result in significant biomechanical improvements using reduced amounts of bone cement (Basafa and Armand, 2014; Santana Artiles and Venetsanos, 2017) as compared to studies where gross filling of the neck and trochanter was employed instead (more than 40–50 ml) (Sutter et al., 2010a). In the optimized injections, cement location was determined utilizing a modified method of Bi-directional Evolutionary Structural Optimization (BESO) (Basafa et al., 2013b). Recent study of Varga et al., however, recommends generalized injection strategies for OHA arguing that detailed preoperative planning and controlled injection techniques are not realistic for the current clinical practice. In their study injection patterns were developed based on the principles of Wolff's law considering how bone would adapt its internal structure to withstand loading of a sideways fall (Varga et al., 2017). Numerical results of Varga's study suggested that cementation of the "main compression bridge" connecting the medial head region of the femur with the greater trochanter provides a larger increase in the yield load and yield energy of the proximal femur in side-way falls as compared to the "single central" configuration (Varga et al., 2017; Beckmann et al., 2007). However, the assumption that a proposed injection strategy can be executed perfectly is not realistic. Therefore, it is also important to consider how the cement diffuses inside the osteoporotic bone structure given any preoperative plan or injection strategy. Our group has previously developed a particle-based hydrodynamic model to predict the infiltration of cement into the porous medium of cancellous bone (Basafa et al., 2013a). This model can be utilized to validate the effectiveness of different augmentation strategies prior to the execution.

In this paper, we investigate if the additional computational overhead of the patient-specific planning can *significantly* improve the bone strength as compared to the novel generic planning attempted in the literature. Other contributions of this paper include: (1) Modifying the computational paradigm introduced by Basafa et al. (2015) to enhance the hydrodynamic simulations; (2) Demonstrating the significance of the hydrodynamic simulation within the context of overall planning paradigm; and (3) Comparing the effect of homogeneous versus inhomogeneous FE models within the proposed overall planning paradigm.

2. Methods

2.1. Plan-based injection

High resolution Computed Tomography (CT) scans from four osteoporotic femur specimens (one male and three females) with average neck t-score of −3.2 (confirming osteoporosis) were obtained. From each pair, one specimen was randomly chosen for augmentation. The new planning paradigm consisted of three phases: (1) Finite Element (FE) optimization of the injection pattern based on the method of BESO; (2) Matching BESO results with realistic injection volumes; and (3) Cement diffusion modeling based on the method of Smoothed Particle Hydrodynamics (SPH) (Basafa et al., 2013a).

To optimize cement pattern, we first created a FE mesh of the femur utilizing concentric rings of quadratic 20-node brick elements, supplemented with 15-node wedge elements at the center (Dhondt, 2004). Next, inhomogeneous material properties were assigned to these elements based on the bone density observed from the pre-operative CT scan. Using linear interpolation of known values for plastic phantom, Hounsfield Unit (HU) intensity values were converted to ash densities. Apparent density was calculated using Eq. (1) were ρ_{ash} and $\rho_{aparent}$ are ash and apparent densities in gr/ml, respectively (van Lenthe et al., 2001).

$$\rho_{aparent} = \rho_{ash} \times 1.79 + 0.119 \tag{1}$$

Finally, the density values were converted to elastic modulus using Eq. (2) (Morgan et al., 2003; Keller, 1994). In these models, the region above the lesser trochanter was assumed to be mostly trabecular bone and the lower region was assumed to be mostly cortical bone. Fig. 1 shows the distribution of elastic modulus of the femora.

$$\begin{aligned} E &= 10,500\rho_{ash}^{2.29} \ \text{Cortical Bone} \\ E &= 6850\rho_{app}^{1.49} \ \text{Trabecular Bone} \end{aligned} \tag{2}$$

where E is the elastic modulus in MPa. The Poisson's ratio of 0.4 is assumed for the femoral bone elements. In the first iteration of the BESO, we populate the proximal part of the femur with PMMA elements with elastic modulus of 1.2 GPa and Poisson's ration of 0.4. The inefficient PMMA elements were gradually removed from the FE model while added to the high load-bearing regions using strain energy as the criterion. Details of the optimization is described elsewhere (Basafa and Armand, 2014) and was previously validated on seven cadaveric experiments (Basafa et al., 2015).

In the second step of planning, we used gradient-descent optimization algorithm to find the closest match to the BESO results through simulation of realistic injection volumes (spheroids) of no more than 10 ml combined. The optimization identifies the lengths (L_i) radii (R_i) of injection blobs in addition to the target point and orientation of the injection path (angles θ *and* φ). A planar schematic of this algorithm is shown in Fig. 2.

$$Max \ \frac{V_{BESO} \bigcap V_{Spheroids}}{V_{BESO} \bigcup V_{Spheroids}} \quad \text{subject to } V_{Spheroids} < 10 \text{ ml} \tag{3}$$

where

$$V_{Spheroids} = \sum_{i=1}^{N} \left(\pi {R_i}^2 L_i + \frac{4}{3} \pi {R_i}^3 \right) \tag{4}$$

and N is the number of spheroids.

In the final step of the planning, we ran the SPH simulation to estimate the final distribution of the cement within the bone structure. SPH incorporates the extreme viscosities associated with the bone cement. This is done by creating a porous model of the proximal femur from CT volume. Assuming an injection rate of 0.1 ml/s and viscosity of 200 Pa·s for the bone cement at the time of injection, SPH simulates the hydrodynamics by removing the tissue particles on the path of a virtual drill (injection line) and gradually introducing cement fluids on the same path (Basafa et al.,

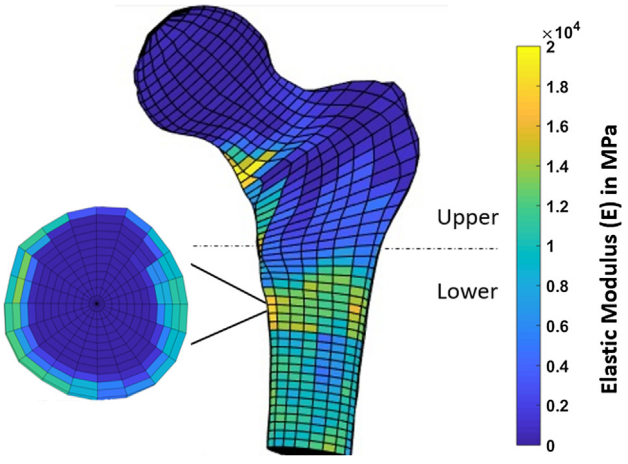

Fig. 1. Distribution of the Young's elastic modulus in the critical region of the femur. Note that the upper region is assumed to be mostly cancellous.

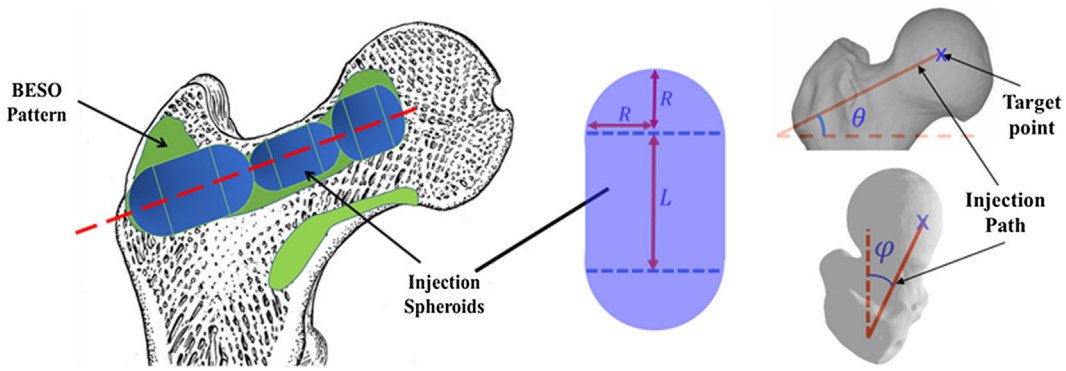

Fig. 2. Schematic of the optimized injection pattern by BESO (green), practical injection volume (blue) and line of injection (red). Note that the target point (starting point of injection), length (L) and radius (R) of each injection blob, and orientation of the injection path are optimally selected to find the closest match between the BESO pattern and injection spheroids. (For interpretation of the references to colour in this figure legend, the reader is referred to the web version of this article.)

2013a). Three major steps of planning paradigm are shown in Fig. 3.

2.2. Generalized injection strategies

In addition to the customized injection strategy, three generalized injection patterns were selected based on the previous studies including the single central (Beckmann et al., 2007) (V1; Red), main compression bridge (V2; Blue) and compression bridge to the lower part of the femoral head (V3; yellow) (Varga et al., 2017). For each of these injections, we assumed a single injection blob (spheroid) with volume of 10 ml connecting the desired anatomical landmarks (Fig. 4). This was followed by a diffusion simulation to estimate the final cement blob utilizing the SPH method described earlier.

2.3. Biomechanical evaluation and data analysis

To evaluate the biomechanical effect of each injection strategy, a static FE analysis was performed on each model using ABAQUS (ABAQUS/Standard V6.8, SIMULIA, Providence, RI). Each model was evaluated with both homogeneous and inhomogeneous material properties to investigate the potential differences of biomechanics when boundary conditions simulating a side-way fall on the greater trochanter are applied (Sutter et al., 2010b) (Fig. 5). For the homogeneous models, we have assumed an average ash density (ρ_{ash}) of 0.206 g/ml for all the bone elements and have calculated the apparent density as 0.488 g/ml from Eq. (1) (van Lenthe et al., 2001). The output parameters from the FE solver included the displacement component of the loaded nodes in the direction of the load and maximum and minimum principal strain values, reported at the centroid of each element. Using the parameters at the load of 500 N and assuming linearity, outputs could be scaled for any desired load. Following the procedure in Basafa et al. (2013b), we define yield load as the load at which combined volume of the failed elements reach 1% of the total volume of the specimen. To compare the effectiveness of different injection strategies, the values of yield load and yield energy were normalized to the non-augmented state of the same specimen for both homogeneous and inhomogeneous models. All generalized injections were considered based on a 10 ml volume of PMMA since the customized injections were constrained by this value in the gradient-descent optimization described before. For each group, mean and standard deviation of the data were given as descriptive statistics. Results of different strategies were compared through a two-way ANOVA test with state significant level of 0.05.

3. Results

To investigate the possibility of realistically reproducing the generalized patterns of injection, we ran SPH for the cement blob of each generalized injection strategy. Fig. 6 shows SPH results of the generalized injections for specimen #1 and the final distribution of cement elements in the FE model. It can be observed from the pattern of the FE mesh that the thickness of PMMA is unlikely to match those of the desired pattern (cylindrical volumes shown in Fig. 4).

All injection methods were found to improve the biomechanical properties of the femur simulating sideway falls. The average injection volume of the optimized pattern was 9.2 ml (SD: 1.0 ml). Most

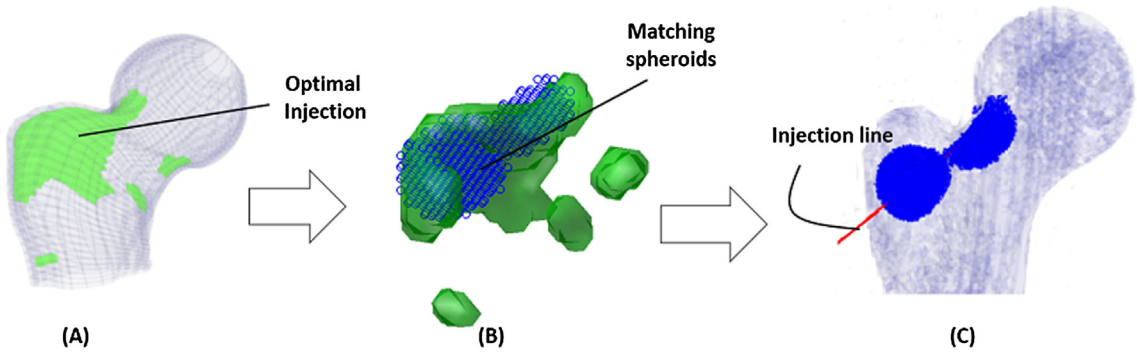

Fig. 3. (A) Schematic of the optimized injection pattern by BESO, (B) the matching spheroids (blue rings) and (C) line of injection with corresponding results of the SPH simulation (blue). (For interpretation of the references to colour in this figure legend, the reader is referred to the web version of this article.)

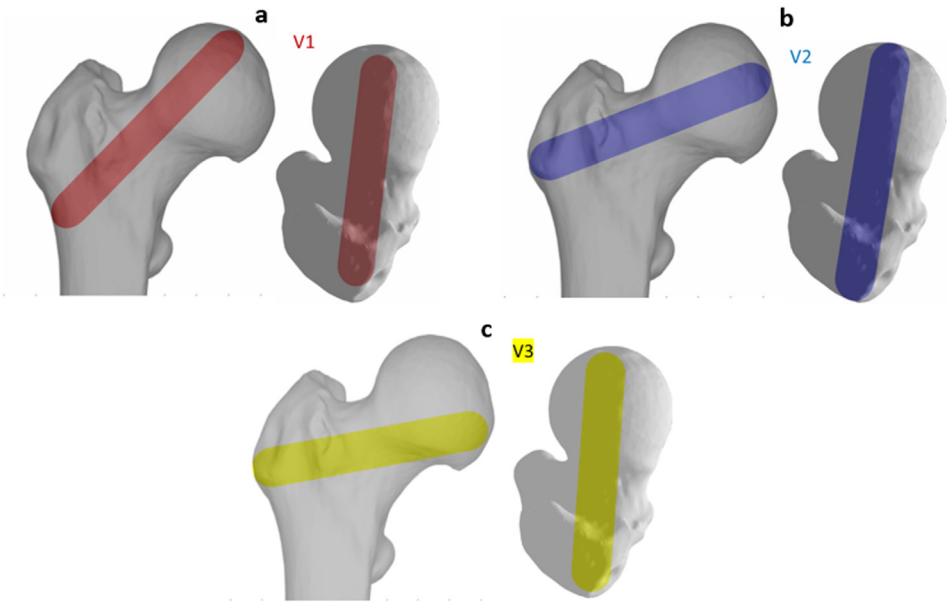

Fig. 4. Generalized injection strategies: a) Single central (V1; Red), b) main compression bridge (V2; Blue) and c) compression bridge to the lower part of the femoral head (V3; yellow). (For interpretation of the references to colour in this figure legend, the reader is referred to the web version of this article.)

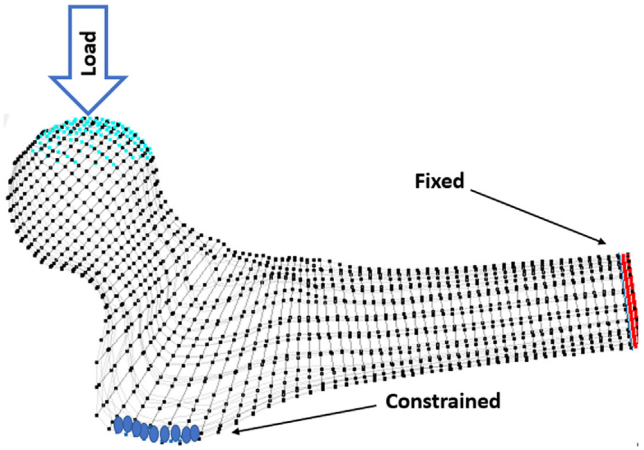

Fig. 5. Boundary conditions simulating a side-way fall on greater trochanter. The distal vertices were fixed in all three directions and the surface vertices on the 10 mm lateral side of the greater trochanter were restricted to move only in the y–z plane.

of the optimal injection lines were directed from the superoanterior aspect of the neck to the posterior of the greater trochanter. Table 1 shows the conversion of SPH results for customized injections patterns into FE mesh.

The normalized Results of the FE analysis suggest that the customized injection patterns are significantly more effective in increasing the yield load of the proximal femur than those of the generalized path in the inhomogeneous models ($P < 0.01$). This difference however is not significant in the homogeneous models ($P = 0.234$). In addition, customized injections can increase the yield energy by 199% (Standard Deviation (SD):78.4%) which is significantly higher than those of generalized injections (117% (SD: 38.4), 140% (SD: 52.6) and 136% (SD: 52.3%) for V1, V2 and V3, respectively). Relative improvements on yield load and yield energy were calculated for all injection variations and are summarized in Figs. 7 and 8. Note that injection in the main compression bridge (V2) is more effective than other variations of the generalized injection.

4. Discussions

Results of the hydrodynamic simulations combined with the FE analyses suggests that OHA can significantly benefit from a preoperative plan that defines the 3D path of the drill hole and pattern of injection as compared to a generalized injection recommendation made in recent literature.

Several cadaveric and simulation-based studies were conducted in the past to evaluate different injection strategies for OHA (Heini et al., 2004; van der Steenhoven et al., 2011; Freitas et al., 2018). In this study, we have investigated four of these strategies: V1; the single central augmentation (Beckmann et al., 2007), V2 and V3 that were previously developed based on the principles of bone remodeling (Wolff's law) and resemble the main compression bridge (Varga et al., 2017), and a modified method of patient-specific OHA based on a previously validated planning paradigm (Basafa and Armand, 2014). Simulation results demonstrated that all injection variations improve the fracture-related biomechanical parameters; however, the customized injection strategy is significantly more effective in improving the fracture-related biomechanical properties of femur compared to all general patterns ($P < 0.01$). In this study, we used both homogeneous and inhomogeneous material properties in FE models to compare different injection strategies. Inhomogeneous model of the bone, which was previously validated in cadaveric studies (Basafa and Armand, 2014) leads to significantly different results from the homogeneous model ($P < 0.01$) suggesting that customized models can greatly benefit OHA, as the mechanical properties of the bone are calculated based on radiodensities of pre-operative CT images.

Computational modeling of novel generalized injection strategies was recently presented by Varga et al. (2017) using nonlinear finite element simulations. Results of this study are similar in concluding that V2 is a more effective than the other two injection strategies. However, this study suggests a lower yield load (32.7% (SD: 15%) compared to about 45%, as reported in the literature) for V2. This difference can be explained by the results of SPH demonstrated in Fig. 6. The desired pattern of PMMA distribution (shown in Fig. 4) is considerably different from post-operative results of the injection. Most of such variations occur in the femoral head and are observed for all generalized injections. In

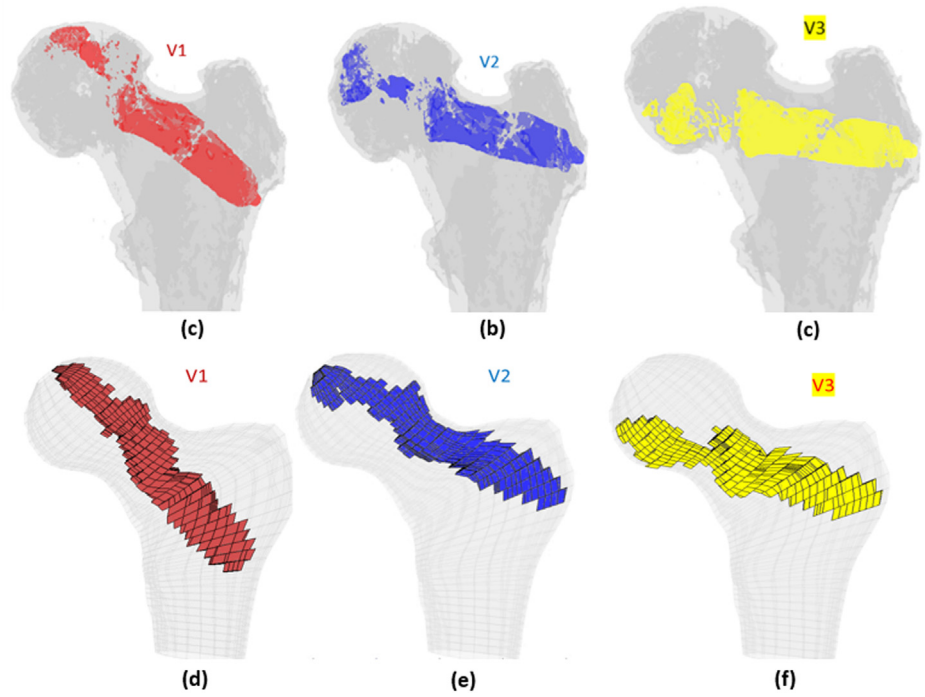

Fig. 6. SPH results of generalized injection strategies (a) the single central mesh of the specimen #1 with diffused volume of cement in different variations of the generalized injection strategies: The single central (V1; Blue), main compression bridge (V2; Blue) and compression bridge to the lower part of the femoral head (V3; yellow). (For interpretation of the references to colour in this figure legend, the reader is referred to the web version of this article.)

Table 1
FE mesh of the femur specimens with the optimized injection patterns after hydrodynamic simulation. Cement volumes were constrained and initially located based on the modified method of BESO (IV: Injection Volume).

#	1	2	3	4
Side	Right	Left	Right	Left
IV (ml)	7.79	9.98	9.87	9.15
Sagittal				
Axial				

addition, unexpected leakage of bone cement combined with exothermic nature of PMMA curing may result in complications such as osteonecrosis or blockage of the blood supply. Thus, once a pattern of injection is chosen for OHA, it is important to consider how PMMA distributes in the proximal femur altering the biomechanical outcomes.

In a more recent study on patient-specific femoroplasty, it was observed that 11.7 ml of cement can lead to 100% increase of yield load in simulation (Santana Artiles and Venetsanos, 2017). Assuming linearity, algorithm presented in this paper increase the yield load by 93.1% for the same volume. However, the injection patterns in the study of Santana et al., are idealized and do not lie on a single line of injection. The proposed modifications to the planning paradigm presented in this paper may reduce this difference since the algorithm decides on a single line of injection for all cases.

Apart from the improved outcome of customized planning for OHA, surgical implementation of this strategy requires an image-guided system for intraoperative feedback. This system consists of surgical navigation involving 2D/3D registration of preoperative CT scans to the femur radiographic images (Otake et al., 2012),

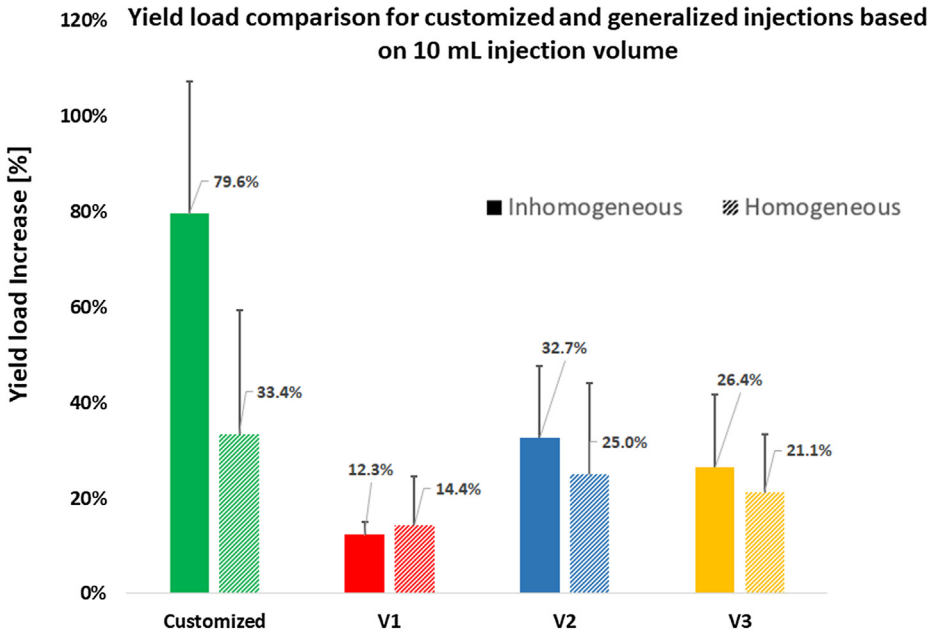

Fig. 7. Percentage of the yield load increase normalized to the non-augmented state of the same specimen.

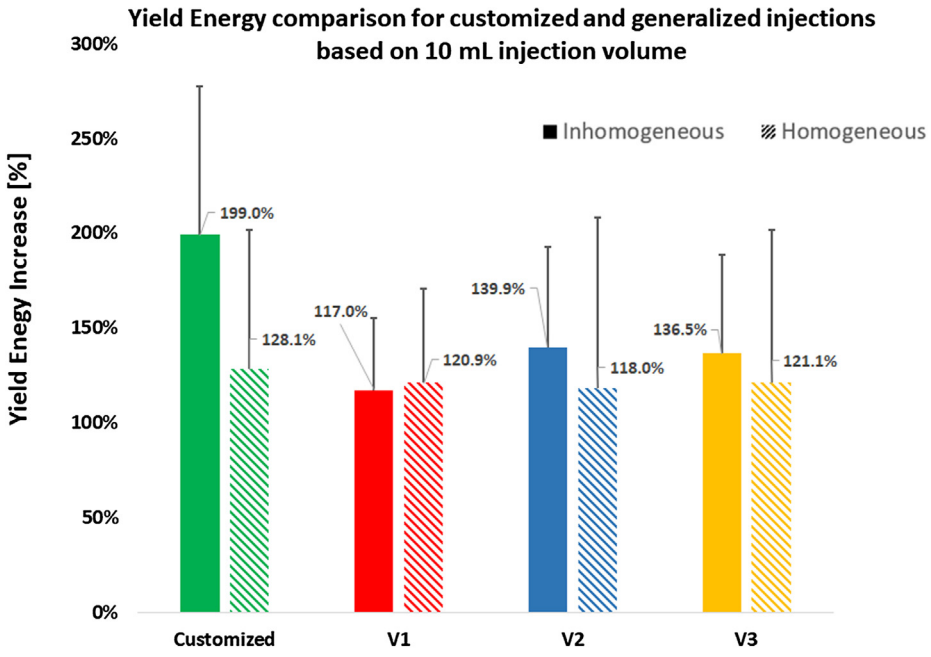

Fig. 8. Percentage of the yield energy increase normalized to the non-augmented state of the same specimen. Among different injection strategies, only the customized injection in the Inhomogeneous group was significantly higher than the others.

real-time tracking, and a handheld motorized bone cement delivery device (Kutzer et al., 2011).

The biomechanical evaluation analysis utilized in this study closely follows the approach that was previously verified against cadaveric experiments where invasive testing was performed to estimate the yield load ($R^2 = 0.74$) (Basafa et al., 2015). However, the future work needs to directly evaluate the modified version of the Basafa's paradigm against cadaveric experiments. Furthermore, this study did not attempt to create a generic approach based on averaging patient-specific approaches. This may or (may not) provide a better generic approach as compared to the present literature. However, applying such generic approaches will still require real-time navigation for trajectory planning, 2D-3D registration, and a motorized device to control the surgical execution. We submit that the main overhead of both generic and patient-specific femoroplasty come from the surgical execution. Thus, the use of a better generic approach may not turn out to offer much advantage compared to the patient-specific paradigm. In addition, since the injections of more than one blob requires controlled injection techniques, all generalized injection were based on a single blob injection (constant rate).

OHA is shown to improve the fracture related biomechanical properties of the femur. However, the exothermic reaction of PMMA polymerization may introduce the risk of thermal necrosis.

This point was not addressed in the current study. In a separate study, we have shown that the maximum temperature-rise of the bone surface is 10 °C which occurs about 12 min after cement injection (Farvardin et al., 2018). Other studies have pointed out that the temperature increase in the range of 45– 60 °C (temperature-rise of 8–23 °C) may cause thermal tissue damage, depending on the exposure time (Diller, 1985; Buettner, 1951). Therefore, in the future, in addition to the mechanical strength of the femur, maximum temperature-rise and duration of thermal exposure are important factors that need to be considered while planning the injection parameters for OHA.

Acknowledgements

We thank Dr. Stephen Belkoff and Mr. Demetries Boston of Johns Hopkins Bayview Medical Center for their help with providing the specimens and the CT scans. This work was supported by grants no. R21 AR063815 and R01 EB0223939 from National Institutes of Health. The efforts of Mr. Farvardin were funded by a JHUAPL graduate fellowship award. The funders had no role in the study design, data collection, analysis of the data, writing of the manuscript, or the decision to submit the manuscript for publication.

Declaration of Competing Interest

None declared.

References

Basafa, E., Murphy, R.J., Kutzer, M.D., Otake, Y., Armand, M., 2013a. A particle model for prediction of cement infiltration of cancellous bone in osteoporotic bone augmentation. PLoS ONE 8 (6), 1.

Basafa, E., Armiger, R.S., Kutzer, M.D., Belkoff, S.M., Mears, S.C., Armand, M., 2013b. Patient-specific finite element modeling for femoral bone augmentation. Med. Eng. Phys. 35 (6), 860–865.

Basafa, E., Armand, M., 2014. Subject-specific planning of femoroplasty: a combined evolutionary optimization and particle diffusion model approach. J. Biomech. 47 (10), 2237–2243.

Basafa, E., Murphy, R.J., Otake, Y., Kutzer, M.D., Belkoff, S.M., Mears, S.C., Armand, M., 2015. Subject-specific planning of femoroplasty: an experimental verification study. J. Biomech. 48 (1), 59–64.

Beckmann, J., Ferguson, S., Gebauer, M., Luering, C., Gasser, B., Heini, P., 2007. Femoroplasty – augmentation of the proximal femur with a composite bone cement – feasibility, biomechanical properties and osteosynthesis potential. Med. Eng. Phys. 29, 755–764.

Buettner, K., 1951. Effects of extreme heat and cold on human skin. II. Surface temperature, pain and heat conductivity in experiments with radiant heat. J. Appl. Physiol. 3 (12), 703–713.

Dhondt, G., 2004. The Finite Element Method of Three Dimensional Thermomechanical Applications. John Wiley & Sons Ltd., Chichester, West Sussex, England.

Diller, Kenneth R., 1985. Analysis of skin burns. In: Heat Transfer in Medicine and Biology. Springer, Boston, MA, pp. 85–134.

Dinah, A.F., 2002. Sequential hip fractures in elderly patients. Injury 33 (5), 393–394.

Eriksson, A.R., Albrektsson, T., 1983. Temperature threshold levels for heat-induced bone tissue injury: a vital-microscopic study in the rabbit. J. Prosthet. Dent. 50 (1), 101–107.

Farvardin, A., Nejad, M.B., Pozin, M., Armand, M., 2018. A Biomechanical and thermal analysis for bone augmentation of the proximal femur pp. V003T04A061–V003T04A061. ASME 2018 International Mechanical Engineering Congress and Exposition, November. American Society of Mechanical Engineers.

Fliri, L., Sermon, A., Wähnert, D., Schmoelz, W., Blauth, M., Windolf, M., 2013. Limited V-shaped cement augmentation of the proximal femur to prevent secondary hip fractures. J. Biomater. Appl. 28 (1), 136–143.

Freitas, A., Silva, L.C.D., Godinho, N.D.V., Farvardin, A., Armand, M., Paula, A.P.D., 2018. Evaluation of a bone reinforcement technique using finite element analysis. Acta ortopedica brasileira 26 (1), 59–62.

Goldacre, M.J., Roberts, S.E., Yeates, D., 2002. Mortality after admission to hospital with fractured neck of femur: database study. BMJ 325 (7369), 868–869.

Heini, P.F., Franz, T., Fankhauser, C., Gasser, B., Ganz, R., 2004. Femoroplasty-augmentation of mechanical properties in the osteoporotic proximal femur: a biomechanical investigation of PMMA reinforcement in cadaver bones. Clinical biomechanics 19 (5), 506–512.

Keller, T.S., 1994. Predicting the compressive mechanical behavior of bone. J. Biomech. 22 (9), 1159–1168.

Kutzer, M.D., Basafa, E., Otake, Y., Armand, M., 2011. An automatic injection device for precise cement delivery during osteoporotic bone augmentation. In: ASME 2011 International Design Engineering Technical Conferences and Computers and Information in Engineering Conference, January. American Society of Mechanical Engineers, pp. 821–827.

Lane, J.M., Russell, L., 2000. Khan NK. Osteoporosis. Clin Orthop 372, 139–150.

Lundskog, J., 1972. Heat and bone tissue. An experimental investigation of the thermal properties of bone and threshold levels for thermal injury. Scand. J. Plast. Reconstr. Surg. 9, 72–74.

Morgan, E.F., Bayraktar, H.H., Keaveny, T.M., 2003. Trabecular bone modulus-density relationships depend on anatomic site. J. Biomech. 36, 897–904.

Otake, Y., Armand, M., Armiger, R.S., Kutzer, M.D., Basafa, E., Kazanzides, P., Taylor, R.H., 2012. Intraoperative image-based multiview 2D/3D registration for image-guided orthopaedic surgery: incorporation of fiducial-based C-arm tracking and GPU-acceleration. IEEE Trans. Med. Imag. 31 (4), 948–962.

Parkkari, J., Kannus, P., Palvanen, M., Natri, A., Vainio, J., Aho, H., Vuori, I., Jarvinen, M., 1999. Majority of hip fractures occur as a result of a fall and impact on the greater trochanter of the femur: a prospective controlled hip fracture study with 206 consecutive patients. Calcif. Tissue Int. 65, 183–187.

Santana Artiles, M.E., Venetsanos, D.T., 2017. A new evolutionary optimization method for osteoporotic bone augmentation. Comput. Meth. Biomech. Biomed. Eng. 20 (7), 691–700.

Sutter, E.G., Wall, S.J., Mears, S.C., Belkoff, S.M., 2010a. The effect of cement placement on augmentation of the osteoporotic proximal femur. Geriatr. Orthop. Surg. Rehab. 1 (1), 22–26.

Sutter, E.G., Mears, S.C., Belkoff, S.M., 2010b. A biomechanical evaluation of femoroplasty under simulated fall conditions. J. Orthop. Trauma 24 (2), 95.

Teng, G.G., 2008. Mortality and osteoporotic fractures: is the link causal, and is it modifiable? Clin. Exp. Rheumatol. 26 (5 0 51), S125.

van Lenthe, G., van den Bergh, J., Hermus, A., Huiskes, R., 2001. The prospects of estimating trabecular bone tissue properties from the combination of ultrasound, dual-energy x-ray absorptiometry, microcomputed tomography, and microfinite element analysis. J. Bone Miner. Res. 16 (3), 550–555.

Varga, P., Inzana, J.A., Schwiedrzik, J., Zysset, P.K., Gueorguiev, B., Blauth, M., Windolf, M., 2017. New approaches for cement-based prophylactic augmentation of the osteoporotic proximal femur provide enhanced reinforcement as predicted by non-linear finite element simulations. Clin. Biomech. 44, 7–13.

van der Steenhoven, T., de Schaasberg, W., Vries, A., Valstar, E., Nelissen, R., 2011. Elastomer femoroplasty prevents hip fracture displacement: in vitro biomechanical study comparing two minimal invasive femoroplasty techniques. Clin. Biomech. 26 (5), 464–469.